Nanodisc-Mediated Conversion of Virustatic Antiviral Antibody to Disrupt Virus Envelope in Infected Cells

Jaehyeon Hwang, Younghun Jung, Seokoh Moon, Seokhyeon Yu, Hyunseok Oh, Soomin Kim, Kyeong Won Kim, Jeong Hyeon Yoon, Jihwan Chun, Sang Jick Kim, Woo-Jae Chung, and Dae-Hyuk Kweon*

Many antibody-based antivirals, including broadly neutralizing antibodies (bnAbs) against various influenza virus strains, suffer from limited potency. A booster of the antiviral activity of an antibody is expected to facilitate development of antiviral therapeutics. In this study, a nanodisc (ND), a discoidal lipid bilayer encircled by membrane scaffold proteins, is engineered to provide virucidal properties to antibodies, thereby augmenting their antiviral activity. NDs carrying the Fc-binding peptide sequence form an antibody-ND complex (ANC), which can co-endocytose into cells infected with influenza virus. ANC efficiently inhibits endosome escape of viral RNA by dual complimentary mode of action. While the antibody moiety in an ANC inhibits hemagglutinin-mediated membrane fusion, its ND moiety destroys the viral envelope using free hemagglutinins that are not captured by antibodies. Providing virus-infected host cells with the ability to self-eliminate by the synergistic effect of ANC components dramatically amplifies the antiviral efficacy of a bnAb against influenza virus. When the efficacy of ANC is assessed in mouse models, administration of ANCs dramatically reduces morbidity and mortality compared to bnAb alone. This study is the first to demonstrate the novel nanoparticle ANC and its role in combating viral infections, suggesting that ANC is a versatile platform applicable to various viruses.

1. Introduction

Antibodies and antibody fragments are a substantial part of treatment approaches against a variety of diseases, including viral infections. Recent antibody engineering technologies, such as antibody drug conjugates (ADCs), Fc engineering, bi-specific antibodies, and immunocytokines, have provided

J. Hwang, Y. Jung, S. Moon, S. Yu, H. Oh, S. Kim, K. W. Kim, J. H. Yoon, J. Chun, W.-J. Chung, D.-H. Kweon
Department of Integrative Biotechnology
Sungkyunkwan University
Suwon 16419, Republic of Korea
E-mail: dhkweon@skku.edu
S. J. Kim
Synthetic Biology and Bioengineering Research Center
Korea Research Institute of Bioscience and Biotechnology
Daejeon 34141, Korea

new opportunities to design antibodies with improved properties to maximize efficacy. However, few therapeutic antibodies have been approved as antiviral agents, except for those urgently required against severe acute respiratory syndrome coronavirus-2 (SARS-CoV-2), whereas many therapeutic antibodies have been marketed, mostly as oncology, autoimmune, and inflammatory therapeutics. This can be due to various reasons, but the limited antiviral efficacy of the antibodies themselves is likely the primary reason for their low success rate.[1]

Antiviral antibodies not only neutralize viruses by interfering with the interaction between virus and host cells by binding to surface proteins such as hemagglutinin (HA), but also help to eliminate antibody-coated infected cells by the immune system effector cells. Viruses can be eliminated completely only by immune cells, whereas the antibody itself transiently reduces virus infectivity by inhibiting viral proteins. Virustatic mode of action and reversible binding of antibodies with viruses are among the reasons for inefficient neutralization and resistance mutations. Furthermore, if not cleared by immune cells, the antibody bound to the virus may facilitate entry of the virus into the target cells through antibody-dependent enhancement (ADE).[2] Thus, we aimed to devise an agent that can provide infected cells with the ability to self-eliminate viruses which invade host cells even in the presence of neutralizing antibodies.

One of the challenges that antibody engineering has been able to address is mutation of the virus. Viruses, especially RNA viruses, exhibit enormous genetic and antigenic diversity.[3] Furthermore, they become resistant to many antivirals because of the high error rate of viral polymerases and selective pressure of drugs.[4] Therefore, numerous studies have been conducted to develop potent broad-spectrum inhibitors against these viruses. Broadly neutralizing antibodies (bnAbs) represent an emerging approach that targets conserved epitopes on viral proteins. The potency of bnAbs has been shown with various viruses, including influenza virus,[5] human immunodeficiency virus (HIV),[6] Ebola virus,[7] and coronavirus.[8] Because mutations in the globular head domain of HA of the influenza virus tend

to allow the virus to escape the host immune response,[9] the stalk domain HA2 with a highly conserved region has mostly been the therapeutic target of bnAbs.[5c,10] Antibodies targeting the globular receptor-binding domain (RBD) of HA or adjacent hypervariable loops can inhibit binding to sialic acid of host cells and act as entry inhibitors.[11] In contrast, bnAbs against the HA stem domain block conformational changes of HA in late endosomes, preventing fusion of the viral membrane.[12] In this study, we employed a bnAb MEDI8852 to demonstrate virus disruption in infected cells because this bnAb has been shown to be effective against a broad range of influenza virus strains.[13]

Nanodisc (ND) is a patch of lipid bilayer where the acyl tails of lipids are encircled with various amphipathic molecules, including membrane scaffold proteins,[14] peptides,[15] and polymers.[16] These discoidal membrane nanostructures have been used to solubilize membrane proteins in a lipid bilayer environment[17] and deliver hydrophobic drugs.[18] Recently, we have shown that NDs carrying a receptor for influenza viruses perforate the viral envelope in the endosome, thereby trapping viral RNA.[19] While liposomes with the same composition merely show a virustatic activity, leading to low neutralizing efficacy, NDs dramatically increase antiviral activity because they physically destroy viruses by utilizing their own invasion machinery, HA. Fusion of a viral envelope with a flat, 2D membrane punctures the virus surface, in contrast to virus-liposome fusion, which does not expose the viral cavity to the environment. Furthermore, ND encircled by membrane scaffold protein (MSP) does not induce not induce no immune response. immune response.[20] Thus, we tested whether a bnAb complexed with a ND would enhance the antiviral potency of the antibody by aiding disruption of the virus in the infected cells. It was shown that the surface area of the ND is crucial for enhancing its antiviral activity. Then, the peptide sequence (Fc-III), capable of high-affinity binding to the Fc region of immunoglobulin (IgG), was inserted into a large-sized end-spliced NDs, resulting in a large Fc-binding ND (FLND).[21] The effect of FLND on the antiviral activity of antibodies was evaluated using MEDI8852 through in vitro and in vivo assays against influenza virus strains.[13] Their modes of action were revealed by determining the intracellular co-localization of the complex with viruses, followed by revealing viral RNA entrapment in endosomes. Based on reduced viral titers and histopathological effects in mice, we suggest antibody-ND complex (ANC) as a potent booster for antiviral activity of bnAbs, which enables the infected cells to digest invading viruses.

2. Results

2.1. Size-Dependent Antiviral Activity of Nanodiscs

As the first step toward antiviral ANCs, NDs were engineered to have better stability and antiviral activity. We reasoned that the surface area of a ND should be sufficiently large to interact with at least a few HA trimers to efficiently induce HA-mediated perforation, as these trimers cooperate for membrane fusion.[22] The cooperation of fusion proteins has also been confirmed in the case of soluble N-ethylmaleimide sensitive

factor attachment protein receptor (SNARE)-driven fusion.[23] Furthermore, it has been shown that the HA trimer involved in receptor binding cannot induce subsequent membrane fusion.[24] A conventional ND made of membrane-scaffold protein MSP1E3D1 (hereafter abbreviated as MSP) has an average diameter of <12 nm and does not provide sufficient surface area for interaction with a sufficient number of trimers with an average diameter of approximately 9 nm (**Figure 1**A).[25]

To test whether the antiviral effect of a ND was proportional to its size, an LND was generated by increasing the length of the MSP, which could be controlled by altering the number of α-helical segments.[26] Therefore, the MSP1E3D1 sequence was repeated, and its end terminals were circularized to form cMSPs (Figure 1B).[27] It has been recently demonstrated that circular NDs, made of cMSPs, offer advantages over conventional NDs in terms of consistency in size and stability against heat.[27b,c] Split-intein-based trans-splicing was used to circularize MSPs because end-splicing occurred inside the cells without the need for a subsequent sortase-mediated circularization process and the separation of linear MSPs from circular MSPs after the reaction. The end-spliced and elongated MSPs (eslMSPs) were formed from a precursor protein of two MSPs flanked by Cfa split inteins,[28] namely CfaN at the C-terminal and CfaC at the N-terminal. Although the size of the precursor protein was expected to be 77.5 kDa, purified proteins appeared at approximately 62.0 kDa on an SDS-PAGE gel, which corresponded to the size of eslMSP with an intein excised after the circularization of the MSP. The eslMSP did not show a reduction in size by the exopeptidase DAPase, confirming the circularization of MSPs through trans-splicing, whereas MSP1E3D1 was shortened by the same treatment, resulting in two bands. (Figure 1C).

Next, MSP1E3D1 and eslMSP were used to assemble conventional NDs and LND, respectively. The lipid-to-protein ratio was 480:1 in the LND and 120:1 in the ND because the surface area was expected to increase fourfold by doubling the length of the MSP. After fractionation of the assembled NDs through size exclusion chromatography (SEC) (Figure S1, Supporting Information), the hydrodynamic diameters of ND and LND were determined to be 12.4 and 25.7 nm, respectively (Figure 1D). Transmission electron microscopy (TEM) images confirmed the enlarged size of the LNDs (Figure 1E).

The reduction of virus-induced cytopathic effects (CPEs) by ND and LND was compared to determine whether the size of the ND was related to its antiviral efficacy. After the incorporation of total ganglioside (TG) into the NDs as the receptor for influenza virus (Figure S2, Supporting Information), they were introduced into the cells infected with the A/Puerto Rico/8/34 (H1N1) influenza virus. LND reduced CPEs very efficiently, with a half-maximal inhibitory concentration (IC_{50}) of 123 nM (Figure 1F). Furthermore, when LND contained a highly purified receptor, GD1a ganglioside (G), the IC_{50} of CPE reduction by LNDG was as low as 2.6 nM (Figure 1G). Thus, we concluded that the size of the ND was a critical determinant of the virucidal effect, leading to an investigation of the relationship between ND size and virus perforation induced by membrane fusion.

A series of experiments were performed to analyze the perforation of the virus envelope by NDs: lipid-mixing assay,

ADVANCED
SCIENCE NEWS
www.advancedsciencenews.com

small
methods
www.small-methods.com
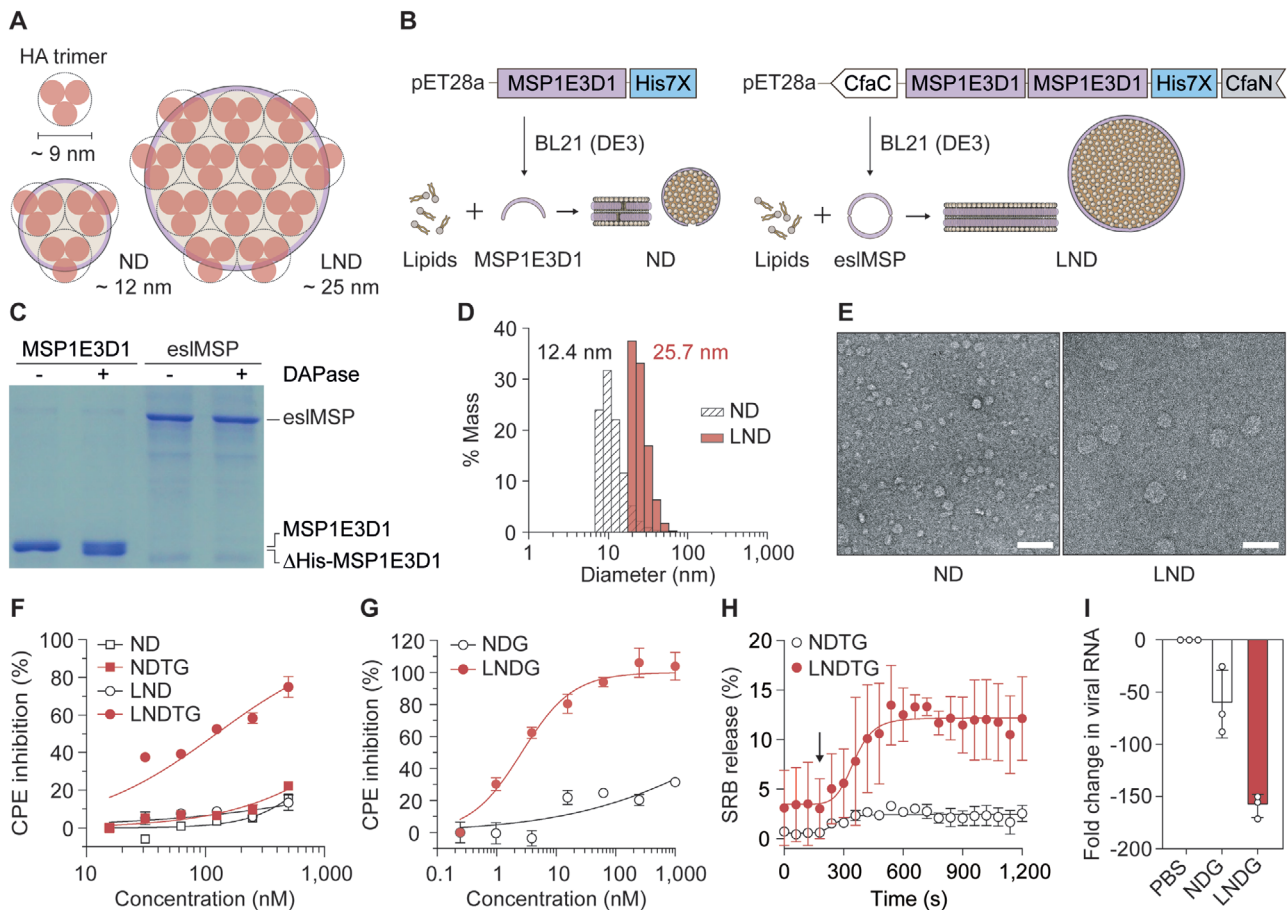
Figure 1. Size-dependent antiviral efficacy of nanodiscs. A) Hypothesis for size-dependent interaction of NDs with HA timers. B) Schematic diagram of the assembly process for ND (left) and LND (right). C) Resistance of linear and circularized MSPs against DAPase digestion, analyzed by SDS-PAGE. D) The average hydrodynamic diameter of ND (12.4 nm) and LND (25.7 nm) measured by dynamic light scattering (DLS) spectroscopy. E) TEM analysis of negatively stained ND and LND. Scale bars: 50 nm. F,G) Size-dependent CPE inhibition against H1N1 influenza virus. H) Time-dependent SRB-release after mixing NDTG or LNDTG with SRB-stained H1N1 virus. Triton X-100 (0.1%, v/v) was used as a positive control. The arrow indicates the time of pH drop. I) RNA accessibility assay. Viral RNA was quantified by qPCR after the virus envelope was perforated with NDs followed by 1 mg L^{-1} RNase treatment for 1 h. Results are expressed as a fold change of viral RNAs compared with those untreated with RNase. Data represent mean ± SD ($n = 3$).

sulforhodamine B (SRB) release assay, RNase A accessibility assay, and TEM. First, the lipid mixing between the ND membrane and influenza virus envelope was analyzed. We added 1,2-dipalmitoyl-sn-glycero-3-phosphoethanolamine-N-(7-nitro-2-1,3-benzoxadiazol-4-yl) (NBD-PE) and 1,2-dipalmitoyl-sn-glycero-3-phosphoethanolamine-N-(lissamine rhodamine B sulfonyl) (Rhod-PE) to the NDs as a fluorescence resonance energy transfer pair, along with 30 mol% TG. After NDs and H1N1 viruses were mixed and equilibrated at 37 °C, the pH was lowered to 5.0 (endosomal pH) using 100 mM citric acid. Both NDs showed similar rates and degrees of lipid mixing (Figure S3, Supporting Information). Lipid mixing occurred upon lowering the pH (Figure S3a, Supporting Information), whereas no apparent lipid mixing was observed at pH 7.4. The fluorescence intensity did not increase in the absence of the influenza virus (Figure S3b, Supporting Information). Thus, the size of NDs did not alter the lipid-mixing kinetics of the ND-virus envelope fusion. Next, we monitored the release of SRB from the influenza virus after labeling with the self-quenching fluorophore SRB (Figure 1H). In contrast to the lipid-mixing assay, the two

NDs showed different rates of SRB release. SRB release by LNDTG was approximately six times faster than that by NDTG after a pH drop. Next, perforation of the envelope was confirmed by measuring the accessibility of RNase (13.5 kDa, 3.8 × 2.8 × 2.8 nm^3) to viral RNA (Figure 1I). After mixing the influenza virus with NDG or LNDG containing 30 mol% ganglioside GD1a, the pH was lowered as described earlier. The samples were treated with 1 mg L^{-1} RNase for 1 h, and the viral RNA was quantified by qRT-PCR. The amount detected after LNDG treatment was 2.6 times lower than that in the NDG-treated group. Both the SRB release assay and RNase accessibility assay suggested that virus envelope perforation was enhanced with an increase in the size of the ND. Finally, TEM images showed that perforation with NDs resulted in the collapse of the virus envelope (Figure S4, Supporting Information). These results suggest that larger NDs facilitated perforation of the viral envelope, leading to stronger antiviral activity of LND than conventional ND.

Although trypsin activates HA allowing the structural rearrangements necessary to fuse with cell membranes, it was

not included in the assays of lipid-mixing, SRB release, RNA accessibility, and immunofluorescence staining because virus stocks used in this study were prepared from eggs, where HA is already activated by egg proteases. However, trypsin was supplemented in the following plaque reduction assay, which requires multiple rounds of infection to form clear plaques. In other words, trypsin was added in the overlay media when viral progenies, which proliferated from infected cells, needed to be activated while it was not included in the reaction buffer when single round fusion event was measured.
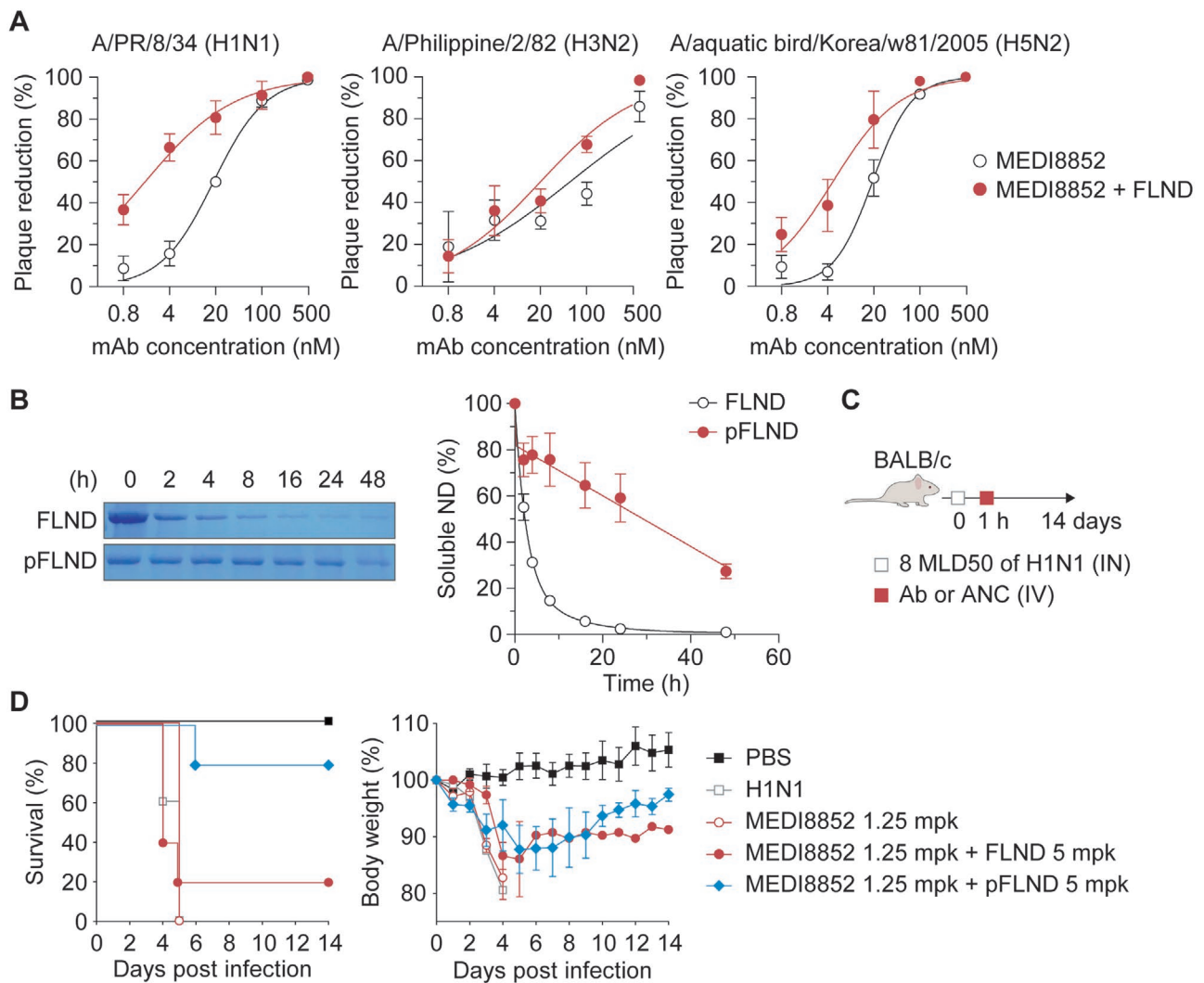
2.2. Preparation of Antibody–Nanodisc Complex

Fc-III, a 13-mer peptide, enables proteins bind to human IgG with a binding constant of 16 nM,[21] but not to mouse or rat IgG isotypes.[29] Fc-III has been shown to endow a fluorescence protein with a long circulation half-life of ≈8 h in mice, a 75-fold increase compared to unmodified fluorescence protein when it is administered with human IgG. Furthermore, Fc-III has been employed in a variety of studies to attach nanoparticles, proteins, and small molecules to antibody.[29] Although off-rate constant between Fc-III with IgG1 predicts a half-life of several minutes, efficient delivery of cargo molecules to target sites in previous studies supports Fc-III-mediated conjugation to IgG1 is likely maintained during circulation. The one-pass circulation time of blood in a mouse has been determined to be approximately 15 s.[30]

Therefore, Fc-III was introduced before the two repeating units of MSPs on eslMSP to provide the ND with an affinity for MEDI8852 (**Figure 2**A and Figure S5, Supporting Information). In addition, flexible linkers (GGGGS) were inserted at each end of Fc-III to avoid steric hindrance between the ND and the antibody. F-eslMSP expressed in Escherichia coli (*E. coli*) (BL21 (DE3)) was purified using a His-tag (Figure S6, Supporting Information). This recombinant protein (F-eslMSP) formed a large ND (Figure 2B–D). The FLND made of F-eslMSP had a lipid composition of 1-palmitoyl-2-oleoyl-sn-glycero-3-phosphocholine (POPC), 1,2-dioleoyl-sn-glycero-3-phospho-L-serine (DOPS),, and cholesterol at a molar ratio of 55:15:30 with a 480:1 lipid-to-protein ratio (Figure 2A). The large size of FLND was confirmed using SEC (Figure 2B), DLS (Figure 2C), and TEM (Figure 2D). FLND has a molecular weight of approximately 900 kDa and a diameter of 23.3 nm.

Next, we investigated whether FLND could bind IgGs. Multiangle light scattering coupled with SEC (SEC-MALS) was performed because the intensity of light scattering (LS) depends on the concentration of macromolecules (Figure 2E).[31] The relative LS intensity of MEDI8852 showed the highest peak at a retention time of 70 min. When MEDI8852 was mixed with FLND at the same molar ratio, the peak of MEDI8852 decreased by more than 80%. Furthermore, the peak disappeared when mixed with MEDI8852 at a 2:1 molar ratio. On the contrary, MEDI8852 did not form complexes with LND, lacking Fc-binding motifs, in a 2:1 molar ratio (Figure S7, Supporting
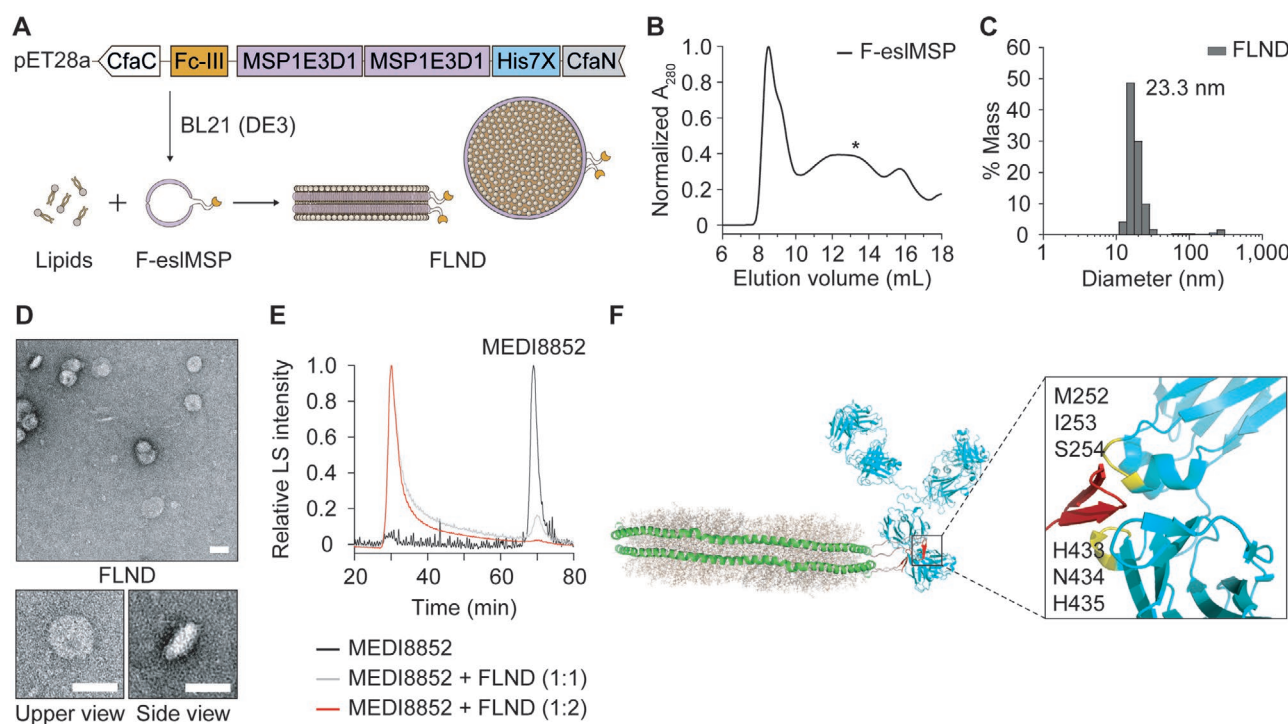
Figure 2. Preparation of antibody-nanodisc complexes. A) Plasmid constructed for expressing F-eslMSP required for FLND assembly. B) Size exclusion chromatography of the assembled FLND with F-eslMSP and lipids. The asterisk denotes the FLND peak. C) DLS histograms of FLND. The average hydrodynamic diameter was estimated to be 23.3 nm. D) TEM analysis of FLND. Scale bar, 25 nm. E) SEC-MALS analysis of antibody-ND complexation at molar ratios between MEDI8852 and FLND 1:0 (black), 1:1 (gray), and 1:2 (red). F) Structural representation of FLND (green and wheat) binding to Fc region of IgGs (cyan). The inter-CH2/CH3 domain (M252, I253, S254, H433, N434, and H435; yellow) of Fc region interacts Fc-III (red) of FLND. The model of IgG-FLND complex is composed of the ND, Fc-III, and antibody, which was modified from PDB IDs 6CLZ, 1DN2, and 1IGT, respectively.

Figure 3. Antibody-nanodisc complexes amplify the antiviral effects of the anti-HA stalk antibody. A) Evaluation of the antiviral activity of MEDI8852 or MEDI8852-FLND by plaque reduction assays against influenza virus strains H1N1 (left), H3N2 (middle), and H5N2 (right). B) A representative SDS-PAGE image. The soluble fraction of FLND or pFLND following incubation with TPCK-treaked trypsin at 37 °C for the designated time-points was subjected to SDS-PAGE analysis (left). Quantification of the band intensity in the SDS-PAGE gel image was performed with Image J (right). A,B) Data represent mean ± SD ($n = 3$) of three independent experiments. C) A schematic for evaluating in vivo antiviral efficacy of the following formulations; MEDI8852, MEDI8852-FLND, and MEDI8852-pFLND. Mice treated with the indicated formulations were monitored daily for 14 days, following inoculation with 8× MLD_{50} of H1N1. D) Kaplan–Meier survival curves (left) and change in body weight (right) of mice. Data represent mean ± SD (5 mice/group).

Information). This result indicates the binding affinity of FLND to MEDI8852 (Figure 2F). Thus, we used a twofold higher concentration of FLND for the preparation of the antibody-ND complex MEDI8852-FLND.

2.3. Amplification of the Antiviral Activity of MEDI8852 by FLND

A bnAb MEDI8852 in scFv-Fc form, where a single-chain variable fragment was fused with the Fc region of IgG1, was prepared (Figure S8, Supporting Information). The antiviral efficacy of MEDI8852, with or without FLND, was evaluated by a plaque reduction assay against three strains of influenza A viruses (H1N1, H3N2, and H5N2) (**Figure** 3A). Each strain of virus

(100 PFU) and inhibitors (MEDI8852 alone or MEDI8852-FLND complex) were mixed, and MDCK cells were treated with this mixture for 1 h. Then, the cells were covered with a DMEM-agarose overlay. Trypsin was included in the overlay media to induce multiple rounds of infection by viral progenies. After 72 h, MEDI8852-FLND showed a 10.9-fold decrease in IC_{50} value compared to MEDI8852 alone (18.6 nM vs. 1.7 nM) against H1N1. When FLND was complexed with MEDI8852, the antiviral efficacy of MEDI8852 against H3N2 and H5N2 also increased, showing 2.8- and 4-times lower IC_{50} values, respectively.

Before testing the in vivo efficacy of FLND, the stability of FLND was improved through PEGylation because it was unstable (Figure S9, Supporting Information) compared with the conventional small NDs. NDs (LND and FLND) were

ADVANCED
SCIENCE NEWS
www.advancedsciencenews.com

small
methods
www.small-methods.com

PEGylated to the cysteine residue of F-eslMSP on its trans-spliced scar using maleimide-functionalized polyethylene glycol. The PEGylated LND and FLND (pLND and pFLND, respectively) showed a significant improvement in stability. The soluble fraction of NDs was analyzed by SDS-PAGE after incubating them at 37 °C for 48 h in the presence of 100 nм trypsin (Figure 3B and Figure S9, Supporting Information). PEGylation effectively reduced digestion by trypsin and the aggregation of NDs. The half-life ($t_{1/2}$) was estimated to be 7.2 h for FLND and 25.7 h for pFLND. After 24 h of incubation, 97% of FLND was cleaved by protease, whereas 60% of pFLND remained undigested.

For the in vivo characterization of ANC, 6-week-old female BALB/c mice were intranasally infected with an $8 \times 50\%$ lethal dose ($8\times$ MLD$_{50}$) of H1N1 (Figure 3C), and after an hour, the mice were administered MEDI8852 alone (1.25 mg kg^{-1}), ANC of MEDI8852-FLND complex (1.25 and 5 mg kg^{-1}, respectively), or ANC of MEDI8852-pFLND complex (1.25 and 5 mg kg^{-1}, respectively) through a single intravenous (IV) injection. The weights of the mice were monitored daily for 14 days postinfection (dpi). The viral titer was lethal enough that none of the mice injected with phosphate-buffered saline (PBS) or MEDI8852 survived after 5 dpi (Figure 3D). In contrast to MEDI8852 alone, MEDI8852-FLND and MEDI8852-pFLND rescued 1 and 4 out of 5 mice, respectively. Mice treated with MEDI8852-pFLND restored most of their body weight loss. The ANC MEDI8852-pFLND could elevate the antiviral efficacy even at lower concentration (0.5 mg kg^{-1} MEDI8852 and 2 mg kg^{-1} pFLND). In contrast, pLND lacking antibody-binding ability did not show such an improvement in the antiviral activity of the antibody (Figure S10, Supporting Information). In addition, the body weight showed no significant difference among the group of mice treated with PBS, 10 mg kg^{-1} pFLND, and 20 mg kg^{-1} pFLND in H1N1-infected mice (Figure S10C, Supporting Information). Furthermore, the MEDI8852-pFLND complex rescued 60% of mice when administered 1 day after infection, while MEDI8852 alone did not increase the survival rate (Figure S11, Supporting Information). These results collectively indicate that pFLND greatly enhances the antiviral effect of MEDI8852 in vitro and in vivo.

2.4. Reduced In Vivo Symptoms and Rapid Recovery by ANC

Histopathological analysis was performed to understand the enhanced antiviral effect of the ANC MEDI8852-pFLND (**Figure 4**). Drugs were injected into mice intravenously 1 h after infection with H1N1 ($4\times$ MLD$_{50}$), and lung tissues were extracted at 6 and 9 dpi for analysis (Figure 4A). Although none of the mice survived at 7 dpi without any treatment, the lower dose of infection allowed some mice to survive after MEDI8852-only treatment. Conjugation of pFLND (2 mg kg^{-1}) with MEDI8852 (0.5 mg kg^{-1}) resulted in a 100% survival rate and the complete recovery of body weight loss (Figure 4B). The ANC MEDI8852-pFLND reduced the lung viral titer by >90% at 6 dpi (Figure S12, Supporting Information). We also observed reduced pulmonary lesions following ANC treatment. Severe pulmonary lesions that could be observed in all treatment groups at 6 dpi were recovered at 9 dpi in mice receiving

the ANC MEDI8852-pFLND (Figure 4C). The recovery from infection was further analyzed by hematoxylin and eosin (H&E) staining of lung tissues. At 6 dpi, infiltration of inflammatory cells, such as monocytes and neutrophils, was observed in the tissues of the infected mice. As the mice began to recover from the viral infection, the peribronchial and alveolar regions in the MEDI8852-pFLND-treated mice showed reduced infiltration of inflammatory cells (Figure 4D). The lung weight of the mice at 6 dpi was measured because viral infection could induce hemorrhagic edema (Figure 4E). There was no significant difference in lung weight between the uninfected group and the MEDI8852-pFLND group, whereas the virus-infected and the MEDI8852-only groups showed 50% and 37% heavier lung weights, respectively. Both MEDI8852 and pFLND were colocalized in the lung alveolar epithelial cells, indicating that the in vivo antiviral efficacy was due to the activity of the ANC MEDI8852-pFLND, which could reach the target cells (Figure 4F). These results suggest that the ANC MEDI8852-pFLND efficiently reduced pulmonary damage caused by viral infection, leading to reduced mortality and morbidity compared to MEDI8852 alone.

We note that nanodiscs, regardless of whether they are composed of MSPs or peptides, are not immunogenic.[18,20] ND alone does not increase total serum levels of IgA, IgM, IgG, and proinflammatory cytokines such as IL-1β, IL-12, IL-6, IFNγ, IL-2, and TNFα in mice immunized with ND. MEDI8852 is a human IgG1 isolated from human memory B cells followed by optimization in vitro for increased potency.[13] Human IgG subclasses have similar relative FcγR-mediated biological activities in mice.[32] MEDI8852 not only directly inhibits HA-mediated membrane fusion it also clears infected cells through the Fc effector functions. Human IgG1 induces antibody-dependent cellular cytotoxicity and antibody-dependent cellular phagocytosis in mouse models. [33] Mixture of MEDI8852 with pLND lacking the ability to bind to the antibody showed in vivo results similar to those by MEDI8852 alone, while ANC formed by pFLND dramatically decreased mortality of mice (Figure S10, Supporting Information). Recently, it has been shown that, 1B07 mAb, a chimeric mouse Fv-human Fc (IgG1) antibody directed to SARS-CoV-2 did not induce pro-inflammatory cytokines and chemokines (IL-6, CCL2, CCL5, CXCL10, CXCL11, IFN-λ, and IFN-β) in bulk lung homogenates from mice compared with the isotype control.[34] Overall, it is not likely that ANC merely played as an immunogen.

2.5. Mode-of-Action of Antibody–Nanodisc complex

The mechanism underlying the enhanced antiviral activity by the ANC MEDI8852-pFLND was investigated. First, MEDI8852-mediated binding of pFLND to the H1N1 virus was analyzed using TEM (**Figure 5**A). While no pFLND was bound to a virion in the absence of antibodies, pFLNDs were observed on the surface of the virus in the presence of MEDI8852, consistent with the SEC-MALS analysis (Figure 2E). Second, MEDI8852-mediated binding of the NDs to influenza virus was further visualized by confocal microscopy (Figure 5B). After 2 h of infection of human lung epithelial (A549) cells with H1N1 virus, the cells were treated with either pFLND or MEDI8852-pFLND
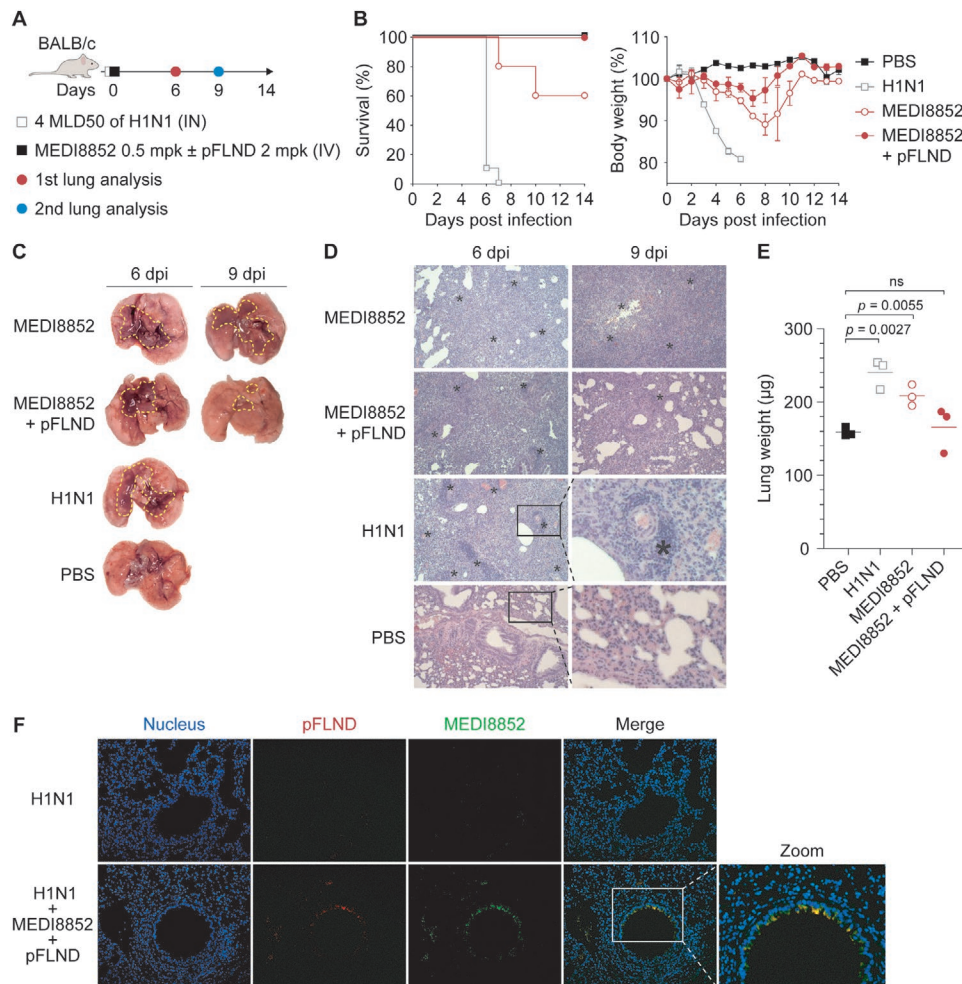
Figure 4. pFLND augments antiviral efficacy of the neutralizing antibody leading to early recovery from lethal influenza virus infection in mice. A) A schematic for evaluating in vivo antiviral efficacy. Mice treated with indicated formulations were monitored daily for 14 days, following inoculation with 4x MLD_{50} of H1N1. B) Kaplan–Meier survival curves (left) and change in body weight (right) of mice. Data represent mean ± SE (10 mice/group) of two independent experiments ($n = 2$). C) Lungs were harvested for evaluating morphological changes. Dashed areas indicate pulmonary lesions. D) Lung tissues were stained by H&E for histopathological evaluation. Asterisks indicate the infiltration of inflammatory cells found in the alveolar space ($\times 100$ magnification). E) Lung weight of H1N1-infected mice. The lungs were excised from each mouse sacrificed at 6 dpi. Data represent mean ± SD ($n = 3$), and p values are shown. F) Fluorescence images of mice lung tissues receiving MEDI8852-pFLND at 6 dpi ($\times 200$ magnification).

for a further 2 h at 37 °C. Both viruses and pFLND (or MEDI8852-pFLND) were primarily present inside the cells at the early stage of infection. While the spots corresponding to pFLND and virus particles were separated from each other in the absence of MEDI8852, they could overlap in the presence of MEDI8852. This result suggests that MEDI8852 not only binds to the virus, but also mediates co-endocytosis of pFLND upon viral infection.

MEDI8852 hinders conformational changes of HA2, leading to the inhibition of membrane fusion between the viral envelope and endosomal membrane.[13] However, NDs utilize membrane fusion to disrupt the virus inside the endosome.[19a] To understand the distinctive antiviral modes of action of ANC, perforation of the viral envelope by the ND was investigated by assaying for the release a self-quenching SRB from the influenza virus. Our results indicated that SRB release was not affected by MEDI8852 alone in the absence of pFLND

(Figure 5C).[35] In contrast, the addition of pFLND in the form of ANC induced SRB release from the virus, indicating viral envelope perforation. It was not surprising that higher perforation was observed at lower MEDI8852 concentrations because membrane fusion was inhibited at higher MEDI8822 concentrations. This result suggests that the mode of action of ANC changes depending on the concentration of the antibody.

Viral envelope perforation results from the fusion pore formed at the final stage of HA2-mediated membrane fusion between the virus membrane and the ND.[19a,36] Because lipid composition is crucial for membrane fusion, $pFLND_{popc}$ composed of 100 mol% POPC was prepared (Figure 5D). Then, its antiviral activity was compared with pFLND containing a negatively charged DOPS and cholesterol, which was the lipid composition employed throughout this study. $MEDI8852-pFLND_{popc}$ showed comparably low enhancement in antiviral activity compared to MEDI8852-pFLND. The IC_{50} values were 30.7 nM
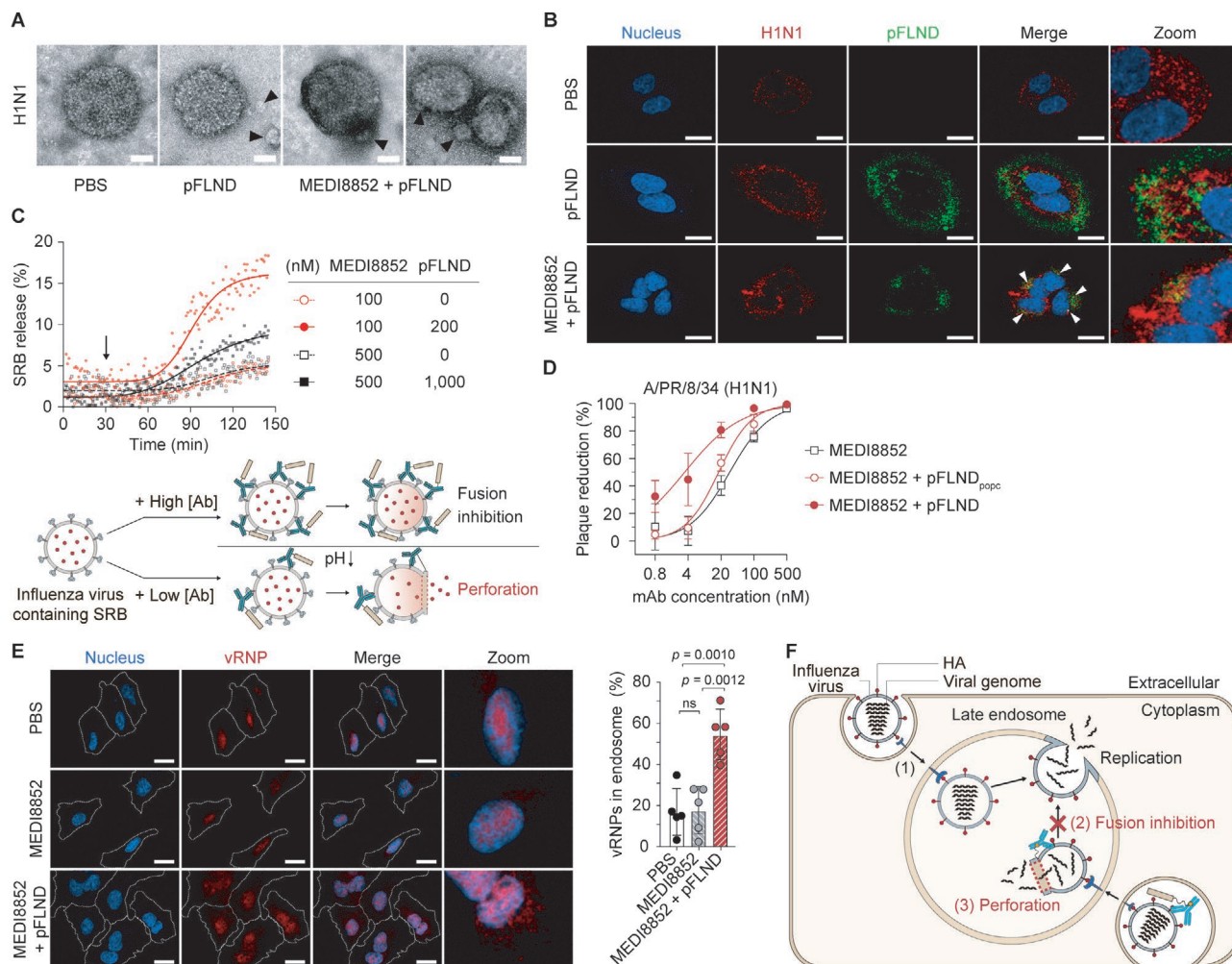
Figure 5. Antibody-dependent perforation of virus envelope by pFLND. A) TEM imaging of pFLND or MEDI8852-pFLND following incubation with H1N1. Black arrows indicate pFLND. Scale bar, 25 nm. B) Immunofluorescence images for the evaluation of the intracellular co-localization of pFLND or MEDI8852-pFLND with influenza virus, 2 h post-infection. The representative images show nuclei stained with Hoechst 33 258 (blue), H1N1 with Alexa Fluor 488 (red), and 1% Rhod-PE (18:1)-labeled pFLND (green). White arrows indicate yellow co-localization spots. Scale bars, 10 μm. C) Time course of SRB leakage from influenza virus upon addition of MEDI8852 or MEDI8852-pFLND (above). Triton X-100 (0.1%, v/v) was used to completely release SRB from viruses. Arrow indicates the time of pH drop. A working hypothesis of switching antiviral mode of action investigated through the release of SRB release from virus by MEDI8852-pFLND (below). At high MEDI8852 concentration, HA2-driven membrane fusion is inhibited, reducing envelope perforation. When HA-mediated fusion is allowed at low MEDI8852 concentration, the fusogenic HA is hijacked by a ND leading to envelope perforation. D) The effect of the lipid composition of ND on membrane fusion was evaluated by plaque reduction assays. Data represent mean ± SD ($n = 3$) from a representative of three independent experiments. E) Confocal microscopy analysis of residual vRNPs (red) of H1N1 in the endosome and nuclei stained with DRAQ5 (blue) (left). Scale bars, 10 μm. Quantitation of vRNPs in the endosome was performed by dividing the intensity of vRNP spots in the endosome by that of intracellular space at 4 h post-infection (right). Data are mean ± SD ($n = 5$), and p values are shown (ns, not significant). F) Mechanism of action of ANC. The influenza virus life cycle (1) is inhibited efficiently by MEDI8852 blocking the conformational change of HA when the antibody concentration is high enough to bind to a large portion of HA molecules (2). If certain HA molecules evade the antibody, which becomes more probable at low antibody concentration, HA can induce membrane fusion with either endosomal membrane or ND. Fusion with the ND of a viral membrane results in vRNA entrapment in the endosome (3). The antibody and nanodisc in an ANC complement each other.

for MEDI8852 alone and 17.9 nM for MEDI8852-pFLND$_{popc}$. In contrast, the IC$_{50}$ of MEDI8852-pFLND was as low as 4.1 nM. The charges of phospholipids and cholesterol are related to the speed and degree of membrane fusion.[37] Thus, we concluded that membrane fusion of NDs with viral membranes leading to envelope perforation is one of the underlying mechanisms of ANC.

Perforation of the influenza virus envelope by NDs leads to the entrapment of viral RNAs in endosomes.[19a] A549 cells

infected with H1N1 were treated with MEDI8852 alone or with the ANC MEDI8852-pFLND. After 4 h of infection, most vRNPs were found in the nucleus of A549 cells when MEDI8852 was used, indicating that fusion inhibition by MEDI8852 could not completely block the endosomal escape of viral RNA. However, MEDI8852-pFLND efficiently trapped vRNPs in late endosomes by perforating the viral envelope, leading to vRNP release into endosomal cavities. We found that approximately half of the vRNPs were trapped in the endosome by MEDI8852-pFLND,

ADVANCED
SCIENCE NEWS
www.advancedsciencenews.com

small
methods
www.small-methods.com

whereas more than 80% of the vRNPs were present in the nucleus after MEDI8852-only treatment (Figure 5E).

In summary, the ANC of a fusion-inhibitory antibody and a ND functionally complemented each other (Figure 5F). When the antibody concentration is sufficiently high to suppress the function of most HA2 molecules, inhibition of membrane fusion and subsequent endosomal escape of the viral genome may protect the cell from infection. However, when there are not enough antibodies to completely hinder HA2 molecules, the evading HA2 can mediate fusion with either the ND or the endosomal membrane. Fusion with NDs results in envelope perforation and entrapment of vRNP in the endosome. In other words, the ND co-delivered with the antibody to the endosome destroys the virus by employing the HA2 molecule that escapes capture by the antibody.

3. Conclusion

Antibody binding to viral surface proteins can interfere with their ability to interact with cell receptors, thereby limiting the ability of the virus to infect cells. In addition, antibodies promote the removal and destruction of the virus or the infected cells by cells of the immune system. In this study, we devised an agent by which the infected cells gained the ability to digest the virus inside the endosome. We demonstrated that an ANC is such an agent. NDs were co-delivered to the infected cell with the antibody. In the endosome, both components of ANC complemented antiviral activity of each other, where mode of actions was switched in the antibody's concentration-dependent manner. While bnAb alone efficiently inhibited membrane fusion at high concentrations, thereby inhibiting virus infection, HA inhibition was not sufficient at low concentrations. We showed that when HA escaped inhibition by the antibody, the ND near the evading HA perforated the viral envelope, thereby complementing antiviral activity. Our results suggest that ANC enables the infected cells to self-digest evading viruses: Antibodies inhibit HA to prevent membrane fusion, while NDs utilize HA-driven membrane fusion to destroy the viral envelope. In conclusion, ANC boosts the efficacy of antiviral antibodies that deserve further attention as a versatile antiviral platform against various viruses.

Although variable antibodies have been employed to treat lung infections, studies have shown that the concentration of therapeutic antibodies in broncheoaveolar lavage fluid (BCLF) is less than a few percent of the antibody in plasma.[38] Poor distribution of IgG into the lung from the systemic circulation may result in the IgG concentration in BCLF lower than IC_{50} of the antibody. Active Ingredient against respiratory syncytial virus (Active Ingredient; $IC_{50} \approx 163–360$ ng mL^{-1}),[39] MEDI8852 against influ-enza ($IC_{50} \approx 41–4050$ ng mL^{-1}),[13,40] and MHAA4549 against influenza ($IC_{50} \approx 195–6765$ ng mL^{-1})[41] show IC_{50}s which can be achieved only at very high plasma concentration. One obvious way to increase the in vivo efficacy of mAb is to lower IC_{50} value. Indeed, the current anti-SARS-CoV-2 mAbs in active preclinical and clinical development have very high potency (IC_{50} values <10 ng mL^{-1} range).[42] Thus, the nanodisc boosting the potency of antiviral activity when mAb concentration was lowered is likely, especially useful for such cases. We note that not only

high-density lipoprotein, which is the origin of nanodisc,[43] but also engineered nanodiscs are able to reach the lung.[19a,44] We also confirmed that pLND could reach the lung well (Figure S13, Supporting Information). This suggests the possibility that ANC may not only enter the lung as associated but also reform in the lung after delivery as dissociated. Our results suggest that ANC amplifies antiviral activity of mAbs through viral envelope perforation in the infected cell even when delivery of mAbs to target sites is limited.

4. Experimental Section

Cells: Madin–Darby canine kidney (MDCK; KCLB, 10034) cells were grown in minimum essential medium (MEM; Hyclone, Logan, UT, USA) supplemented with 10% fetal bovine serum (FBS; Sigma-Aldrich, St. Louis, MO, USA), 100 U mL^{-1} of Active Ingredient G, 100 µg mL^{-1} of Active Ingredient, and 0.25 µg mL^{-1} Active Ingredient B (Hyclone). Human epithelial lung carcinoma A549 (A549; KCLB, 10185) cells were cultivated in Roswell Park Memorial Institute 1640 medium (RPMI; Hyclone) containing the same supplements as MDCK cell medium. The cells were grown at 37 °C in a 5% CO$_2$ humidified incubator and were passaged once they reached 80–90% confluence. Human embryonic kidney (HEK) 293F (Invitrogen, Carlsbad, CA, USA) cells were cultured in FreeStyle 293 expression medium (Invitrogen) in a humidified 37 °C shaking incubator at 125 rpm with 8% CO$_2$. HEK 293F cells are typically subcultured when they reach a final density of $2–3 \times 10^6$ viable cells mL^{-1}.

Viruses: Influenza virus strains A/Puerto Rico/8/34 (H1N1), A/Sydney/5/97 (H3N2), A/X31 (H3N2), A/Philippine/2/82 (H3N2), and A/aquatic bird/Korea/w81/2005 (H5N2) were propagated in 10-day-old embryonated eggs at 37 °C and 50% humidity with 1000 PFU of each virus. After 2–3 days, the allantoic fluid was harvested, and the viruses were isolated using a 50%, 40%, 30%, and 20% w/v sucrose gradient in PBS. Viral titers were determined by plaque assays in MDCK cells.

Preparation of Antibodies: The human MED8852 plasmid sequence was obtained from a previous study.[13] The scFv-Fc MEDI8852 plasmid (125 µg) was transiently transfected into 200 mL of HEK293F cells (1×10^6 cells mL^{-1}) with a DNA:PEI ratio of 1:3 using PEImax (Polyscience, Inc., Warrington, FL, USA) in the culture medium. After 72 h, the culture medium was centrifuged at $6000 \times g$ for 10 min, and the supernatant was purified with Protein G resin. Purified proteins were analyzed by SDS-PAGE and a dot blot assay.

MSP Expression and Purification: MSP-related proteins were prepared as previously reported.[19a] Briefly, *E. coli* (BL21 (DE3)) were disrupted using a high pressure homogenizer Nanogenizer (Genizer LLC, Irvine, CA, USA), and the proteins were purified using Ni-NTA agarose beads, and excess imidazole was removed using a PD-10 desalting column. Purified proteins were stored at −80 °C with 10% v/v glycerol for long-term storage. Protein concentration was determined using a detergentcompatible protein assay (Bio-Rad, Hercules, CA, USA) with bovine serum albumin (BSA) as the standard, and purity was confirmed by SDS-PAGE. For in vivo studies, the endotoxin of proteins was removed using 0.5 mL Pierce High Capacity Endotoxin Removal Spin Column (Thermo Fisher Scientific, Waltham, MA, USA).

Nanodisc Preparation: NDs were prepared as previously described.[19a] Typically, the molar ratio of phospholipids and gangliosides was 100:0 for empty discs or 70:30 for ganglioside-embedded nanodiscs, and the lipid composition was adjusted as needed. NDs containing ganglioside were assembled using 70 mol% POPC and 30 mol% TG or GD1a. Nanodiscs to measure lipid mixing contained 1.5 mol% NBD-PE and Rho-PE. For FLNDs, 55 mol% POPC, 15 mol% DOPS, and 30 mol% cholesterol were mixed. All phospholipids and TG were purchased from Avanti Polar Lipids (Alabama, USA). Ganglioside GD1a was purchased from Cayman Chemical (Ann Arbor, USA). Lipid mixtures prepared at the desired molar ratio were treated with nitrogen gas to evaporate the solvents, followed by vacuum overnight. The resultant lipid film was hydrated

with ND assembly buffer (10 mm Tris/HCl, 100 mm NaCl, 0.5 mm EDTA, 50 mm sodium cholate, pH 7.4). After sonication of the lipid-detergent solution at 55 °C for 30 min, each MSP was added to the solution. SM-2 bio-beads (Bio-Rad) were added to the mixture at 4 °C for 5 h to remove the detergent. The NDs were purified by size exclusion chromatography using a Superose 6 increase 10/300 GL column (GE Healthcare, Uppsala, Sweden). Fractions corresponding to the size of each ND were collected and concentrated using an Amicon Ultra (10 kDa cutoff) centrifugal filter (EMD Millipore, Billerica, MA, USA).

Light Scattering: The hydrodynamic diameter and size distributions of NDs were measured using a DynaPro NanoStar DLS instrument (WyattTechnologies, Goleta, CA, USA), followed by analysis using the instrument software (Dynamics version 7.0).

Electron Microscopy: The negative staining procedure was slightly modified from previously described protocols.[19a] Ten microliters of the sample were placed on carbon-coated gold grids (TED PELLA, Inc., Redding, CA, USA) for 1 min, and the excess sample was removed by blotting with a filter paper. Next, the grids were washed with 10 μL ultrapure water and stained with 5 μL of 1% w/v uranyl acetate for 20 s. During the procedures, excess liquid was removed with filter paper. The prepared grids were air-dried until TEM analysis was performed. All specimens were analyzed by energy-filtering TEM using a JEM 3010 microscope (JEOL Ltd., Tokyo, Japan), which was operated at an accelerating voltage of 300 kV.

Pull-Down Assay: Ni-NTA agarose beads equilibrated with washing buffer (5 mm imidazole in PBS, pH 7.4) were incubated with NDs at 4 °C for 2 h with rotation. Next, the ND–bead complexes were treated with 1×10^8 PFU of H1N1 virus at 4 °C for 2 h with rotation. Next, the H1N1 bound to beads was eluted with elution buffer (500 mm imidazole in PBS, pH 7.4), followed by washing three times to remove unbound viruses. After removing excess imidazole from the elute with an Amicon Ultra (10 kDa cutoff) centrifugal filter, H1N1 was detected using dot-blot assays as described below.

Dot Blot Assay: Five microliters of each virus were spotted on a nitrocellulose blotting membrane (GE Healthcare). The blotted viruses dried for 1 h and washed with tris-buffered saline-tween (TBST) (10 mm Tris/HCl, 150 mm NaCl, 0.05% v/v Tween-20, pH 8.0) three times. After blocking with blocking buffer (TBST containing 0.5% BSA) for 1 h, anti-influenza A virus H1N1 HA monoclonal antibody (BioRad) or scFv-Fc MEDI8852 in blocking buffer was incubated for 1 h with constant shaking. The membranes were washed three times (10 min each) with TBST and then incubated with horseradish peroxidase-conjugated goat anti-mouse (or anti-human) IgG secondary antibodies (Sigma-Aldrich) diluted in blocking buffer for 1 h. After washing three times (10 min each) with TBST, the membranes were visualized by chemiluminescence with WESTSAVE Gold (Young In Frontier Co., Seoul, Korea). All the procedures were carried out at 25 °C.

CPE Inhibition: MDCK cells were seeded at a density of 2.0×10^4 cells/well into 96-well plates and allowed to adhere for 24 h at 37 °C in 5% CO₂. NDs were mixed with diluted A/Puerto Rico/8/34 (H1N1) virus (multiplicity of infection, (MOI = 0.05) at designated concentrations for 1 h at 37 °C. After removing the growth medium, the cells were washed twice with PBS and infected with ND- or LND-treated virus. After 18 h of incubation at 37 °C and 5% CO₂, the medium was discarded, and the cells were fixed with 4% formaldehyde. The cells were then stained with 0.5% crystal violet for 1 h at 25 °C. After methanol extraction, CPE was examined by measuring the absorbance at 570 nm with a Synergy H1 spectrophotometer (Biotek, Winooski, VT, USA).

Lipid-Mixing Assay: Membrane fusion between the ND and viral envelope was verified by a lipid mixing assay, a commonly used method to study fusion. The NDs were labeled with NBD-PE and Rhod-PE (1.5 mol% of each was added to 97 mol% POPC), and virus fusion was monitored by dequenching NBD fluorescence (excitation at 465 nm and emission at 530 nm) using a Spectramax M2 spectrophotometer (Molecular Devices, Sunnyvale, CA, USA). The virus (630 μm total viral protein) was mixed with target NDs (70 μm total lipid) in a 384-well white plate, and then the temperature of the mixture was equilibrated at 37 °C for 30 min. Fusion was triggered by acidification to pH 5.0,

using 100 mm citric acid. After 90 min, 0.1% Triton X-100 was added to the mixture to obtain the maximum intensity of NBD when it was fully diffused into the solution. Lipid mixing values were collected and normalized as follows: $F = (F_{obs} - F_0)/(F_{max} - F_0)$, where F_{obs} is the observed fluorescence intensity, F_0 is the fluorescence value before acidification, and F_{max} is the fluorescence intensity after the addition of Triton X-100.

SRB Release Assay: A/Puerto Rico/8/34 (H1N1) viruses were mixed with 2X volume of 20 mm SRB for 20 h at 25 °C to stain the internal space of the virions. Free SRB dye was then removed using a PD Minitrap G-10 desalting column. All the experimental procedures were performed at 37 °C. Briefly, viruses were mixed with each sample (nanodisc, MEDI8852, or ANC) for 30 min at 37 °C before lowering the pH. After a pH drop with 100 mm citric acid, fluorescence changes were measured at ex/em of 550/590 nm using a spectrophotometer (Spectramax M2).

RNA Accessibility Assay: Briefly, 20 μL of H1N1 (26 mg L⁻¹) were mixed with 10 μL of PBS or 750 nm of each ND for 15 min at 37 °C. Subsequently, the mixture was supplemented with 2 μL of 65 mm citric acid to lower the pH to 5.0, followed by further incubation for 20 min at 37 °C. For the degradation of vRNA, each mixture was exposed to 2 μL of RNase A (GeorgiaChem, Norcross, GA, USA) (17 mg L⁻¹) and incubated for 1 h at 25 °C. To measure undegraded vRNA, reverse transcription (RT)-PCR was carried out using M-MLV reverse transcriptase (ELPIS-BIOTECH, Inc., Daejeon, Korea) with primers for the viral M gene of A/Puerto Rico/8/34; 5-TGCACTTTGACATTGTGGATTCTTG-3 and 5-CCCTCATAGACTTTGGCACTCC-3'. The coding region of the M sequence in the RT product was amplified with the described primers by using HiPi Real-Time PCR 2x Master Mix (ELPIS-BIOTECH) under the following thermal cycling conditions: 45 cycles at 95 °C for 5 s, 56 °C for 10 s, and 72 °C for 30 s. All experiments were performed in triplicate, and the fold change was calculated using the ΔCt method.

SEC-MALS: A DAWN 8+ multi-angle light scattering detector with an Optilab T-rEX refractometer (Wyatt Technology, Santa Barbara, CA, USA) was combined with a high performance liquid chromatography (Waters Corporation, Milford, MA, USA) equipped with Superose 6 increase 10/300 (GE) SEC column and a refractive index (RI) detector. Data collection and analysis were performed using ASTRA 6.1 software (Wyatt Technology). The dn/dc (refractive index increment) value was defined as 0.185 mL g⁻¹. All experiments were performed at room temperature.

Plaque Reduction Assay: The number of plaques was analyzed to assess antiviral activity. MDCK cells were seeded at a density of 1.2×10^6 cells/well into six-well plates and allowed to adhere for 24 h at 37 °C in 5% CO₂. Each inhibitor was mixed with 100 PFU of each influenza virus strain at 37 °C for 1 h. After two washes with PBS, the cells were treated with a mixture of virus and inhibitor at 37 °C for 1 h. Next, the infected cells were washed with PBS and 2 mL of agarose overlay medium consisting of 1% w/v agarose, $1 \times$ Dulbecco's modified Eagle's medium, and 1 μg mL⁻¹ tosyl phenylalanyl chloromethyl ketone (TPCK)-treated trypsin was added to each well. The plates were incubated at 37 °C in 5% CO₂ for 3 days, fixed with 4% formaldehyde, and stained with 0.5% w/v crystal violet.

PEGylation of Nanodiscs: PEGylation is performed via the maleimide-thiol bond between 1,11-bismaleimido-triethyleneglycol (BM(PEG)3) and a cysteine scar at the splice junction. First, NDs were mixed with tris (2-carboxyethyl)phosphine hydrochloride (TCEP-HCl) at a final concentration of 5 mm for 30 min, followed by removal of TCEP through buffer exchange using PD-10 desalting columns. Next, a 20-fold molar excess of BM(PEG)3 dissolved in dimethyl sulfoxide was added to the proteins and incubated for 1 h. Next, dithiothreitol (DTT) was added at a final concentration of 10 mm to stop reaction, and the mixture was incubated for 15 min. Then, PD-10 desalting columns were used to remove the DTT. All the procedures were conducted 25 °C.

Trypsin Resistance Tests: The procedure used for the proteolytic digestion of NDs with trypsin was modified from a previously described protocol.[45] Briefly, 3 μm NDs in PBS were incubated with 100 nm of TPCK-treated trypsin at 37 °C for the indicated time. Digested samples were centrifuged at $10\,000 \times g$ for 10 min, and the soluble fractions were

analyzed by SDS-PAGE. GelAnalyzer software (GelAnalyzer 2010a by Istvan Lazar, www.gelanalyzer.com) was used to quantify the gel images.

Animals: Six-week-old female BALB/c mice (Koatech, Inc., Pyeongtaek, Korea) were infected intranasally with two- or fourfold 50% mouse lethal dose ($4 \times$ MLD$_{50}$) of A/PR/8/34 H1N1 virus (50 PFU or 100 PFU). Mice were then intravenously administered once with each drug at the indicated times. Body weight was measured daily, and survival was evaluated. In addition, the lung tissues of mice from each group were harvested on days 6 and 9, weighed, and homogenized in PBS to determine viral titers using a plaque assay. When a mouse lost more than 20% of its initial body weight, it was defined as dead and humanely killed. The remaining mice were sacrificed at the end of the experiment 14 days post-infection. All animal experiments complied with the policies of the Institutional Animal Care and Use Committee of Sungkyunkwan University (IACUC number: SKKUIACUC2021-01-47-1).

Immunofluorescence Staining: For colocalization analysis, the NDs were labeled with Rhod-PE (18:1) (Avanti Polar Lipids, Inc., Alabaster, AL, USA) and mixed with MEDI8852, followed by incubation with H1N1 for 1 h. A549 cells were inoculated with the mixture (MOI = 0.1) at 37 °C for 2 h. After incubation, the cells were fixed with 3.7% formaldehyde in PBS for 15 min and permeabilized with 0.5% Triton X-100 in PBS for 5 min. After blocking with 3% BSA in PBS (blocking buffer), the fixed cells were treated with mouse anti-H1N1 HA monoclonal antibody (1:500 dilution) (Abcam, Cambridge, UK) in blocking buffer for 1 h. After washing three times with PBS, the cells were treated with Alexa Fluor 488-conjugated goat anti-mouse antibody (1:200 dilution) (Invitrogen) in blocking buffer for 1 h. After washing three times with PBS, the cells were stained with Hoechst 33258 (1:500 dilution; Invitrogen) for 5 min and mounted with ProLongTM Diamond Antifade Mountant (Molecular Probes, Eugene, OR, USA). To quantify vRNP entrapment, A549 cells were inoculated with 1000 PFU of H1N1 (MOI = 0. 01) for 1 h following mixing with PBS, MEDI8852 (500 nм), or MDI8852-NDs (500 nм and 1 μм, respectively) for 1 h to quantify the amount of vRNPs in endosomes. After the inoculums were washed with PBS, the cells were treated with RPMI medium and incubated at 37 °C. At 4 h post-infection, the cells were treated as described above, except that the primary antibody was reacted with mouse anti-NP monoclonal antibody (1:200 dilution) (Abcam), and nuclei were stained with DRAQ5 (1:500 dilution) (Invitrogen). All images were acquired using a Leica TCS SP8 HyVolution confocal microscope with a $40 \times$ objective (HC PL APO $40 \times$ /1.10 W CORR CS2, FWD = 0.65 mm; Leica Microsystems, Wetzlar, Germany), and the images were processed identically.

Histopathological Staining: Lung tissues harvested from the mice euthanized on days 6 and 9 in each group were weighed, fixed in 10% buffered formalin, dehydrated, and embedded in paraffin wax. Sections (5 μm) were mounted on slides, and histopathological changes were examined by H&E staining.

For immunofluorescence analysis, 5 μm thick tissue sections were washed with PBS and blocked with PBS containing 10% FBS and 0.2% Triton X-100 for 1 h. The sections were stained with polyclonal rabbit His-tag antibody (1:200 dilution) (Invitrogen) for the His-tag of MSP-related proteins, followed by goat anti-rabbit IgG Alexa Fluor 594 secondary antibody (1:200 dilution) (Invitrogen) and goat anti-human IgG Fc FITC (1:200 dilution) (Abcam) to detect MEDI8852. The cells were then incubated with Hoechst 33258 (1:500 dilution; Invitrogen) at 25 °C for 5 min, followed by mounting with ProLongTM Diamond Antifade Mountant (Molecular Probes). Images were acquired using a Zeiss LSM 700 confocal microscope at a magnification of $200 \times$.

In Vivo Biodistribution of Nanodiscs: Nanodisc was labeled with lipophilic DiR fluorophore (Thermo Fisher Scientific) before injection. Then, Balb/c mice were intravenously administered 50 μg of ND-DiR. After 1 day, the mice were euthanized and the heart, lung, liver, spleen, and kidney were removed. DiR fluorescence intensity was measured using the IVIS Lumina XR (Caliper Life Sciences, Hopkinton, MA, USA).

Statistics: No statistical methods were used to determine sample size. All statistical analyses were performed using GraphPad Prism software (GraphPad Software Inc., San Diego, CA, USA). Statistical significance was determined using the Student's t-test. Statistical significance was set at $p < 0.05$.

Supporting Information

Supporting Information is available from the Wiley Online Library or from the author.

Conflict of Interest

The authors declare no conflict of interest.

Data Availability Statement

The data that support the findings of this study are available from the corresponding author upon reasonable request.

[1] a) Z. Elgundi, M. Reslan, E. Cruz, V. Sifniotis, V. Kayser, *Adv. Drug Delivery Rev.* **2017**, *122*, 2; b) S. Ahangarzadeh, Z. Payandeh, R. Arezumand, K. Shahzamani, F. Yarian, A. Alibakhshi, *Int. Immunopharmacol.* **2020**, *86*, 106760; c) K. Tao, P. L. Tzou, J. Nouhin, H. Bonilla, P. Jagannathan, R. W. Shafer, *Clin. Microbiol. Rev.* **2021**, *34*, e00109.

[2] K. L. Winarski, J. Tang, L. Klenow, J. Lee, E. M. Coyle, J. Manischewitz, H. L. Turner, K. Takeda, A. B. Ward, H. Golding, *Proc. Natl. Acad. Sci. USA* **2019**, *116*, 15194.

[3] a) J. Holland, K. Spindler, F. Horodyski, E. Grabau, S. Nichol, S. VandePol, *Science* **1982**, *215*, 1577; b) A. S. Lauring, J. Frydman, R. Andino, *Nat. Rev. Microbiol.* **2013**, *11*, 327.

[4] a) E. Vanderlinden, L. Naesens, *Med. Res. Rev.* **2014**, *34*, 301; b) K. K. Irwin, N. Renzette, T. F. Kowalik, J. D. Jensen, *Virus Evol.* **2016**, *2*, vew014.

[5] a) D. C. Ekiert, G. Bhabha, M. A. Elsliger, R. H. Friesen, M. Jongeneelen, M. Throsby, J. Goudsmit, I. A. Wilson, *Science* **2009**, *324*, 246; b) D. C. Ekiert, R. H. Friesen, G. Bhabha, T. Kwaks, M. Jongeneelen, W. Yu, C. Ophorst, F. Cox, H. J. Korse, B. Brandenburg, R. Vogels, J. P. Brakenhoff, R. Kompier, M. H. Koldijk, L. A. Cornelissen, L. L. Poon, M. Peiris, W. Koudstaal, I. A. Wilson, J. Goudsmit, *Science* **2011**, *333*, 843; c) C. Dreyfus, N. S. Laursen, T. Kwaks, D. Zuijdgeest, R. Khayat, D. C. Ekiert, J. H. Lee, Z. Metlagel, M. V. Bujny, M. Jongeneelen, R. van der Vlugt, M. Lamrani, H. J. Korse, E. Geelen, O. Sahin, M. Sieuwerts, J. P. Brakenhoff, R. Vogels, O. T. Li, L. L. Poon, M. Peiris, W. Koudstaal, A. B. Ward, I. A. Wilson, J. Goudsmit, R. H. Friesen, *Science* **2012**, *337*, 1343.

[6] a) T. Zhou, I. Georgiev, X. Wu, Z. Y. Yang, K. Dai, A. Finzi, Y. D. Kwon, J. F. Scheid, W. Shi, L. Xu, Y. Yang, J. Zhu,

ADVANCED
SCIENCE NEWS

www.advancedsciencenews.com

small
methods

www.small-methods.com

M. C. Nussenzweig, J. Sodroski, L. Shapiro, G. J. Nabel, J. R. Mascola, P. D. Kwong, *Science* **2010**, *329*, 811; b) E. Falkowska, K. M. Le, A. Ramos, K. J. Doores, J. H. Lee, C. Blattner, A. Ramirez, R. Derking, M. J. van Gils, C. H. Liang, R. McBride, B. von Bredow, S. S. Shivatare, C. Y. Wu, P. Y. Chan-Hui, Y. Liu, T. Feizi, M. B. Zwick, W. C. Koff, M. S. Seaman, K. Swiderek, J. P. Moore, D. Evans, J. C. Paulson, C. H. Wong, A. B. Ward, I. A. Wilson, R. W. Sanders, P. Poignard, D. R. Burton, *Immunity* **2014**, *40*, 657; c) C. K. Wibmer, P. L. Moore, L. Morris, *Curr. Opin. HIV AIDS* **2015**, *10*, 135.

[7] a) J. Misasi, M. S. Gilman, M. Kanekiyo, M. Gui, A. Cagigi, S. Mulangu, D. Corti, J. E. Ledgerwood, A. Lanzavecchia, J. Cunningham, J. J. Muyembe-Tamfun, U. Baxa, B. S. Graham, Y. Xiang, N. J. Sullivan, J. S. McLellan, *Science* **2016**, *351*, 1343; b) X. Zhao, K. A. Howell, S. He, J. M. Brannan, A. Z. Wec, E. Davidson, H. L. Turner, C. I. Chiang, L. Lei, J. M. Fels, H. Vu, S. Shulenin, A. N. Turonis, A. I. Kuehne, G. Liu, M. Ta, Y. Wang, C. Sundling, Y. Xiao, J. S. Spence, B. J. Doranz, F. W. Holtsberg, A. B. Ward, K. Chandran, J. M. Dye, X. Qiu, Y. Li, M. J. Aman, *Cell* **2017**, *169*, 891; c) L. B. King, B. R. West, C. L. Moyer, P. Gilchuk, A. Flyak, P. A. Ilinykh, R. Bombardi, S. Hui, K. Huang, A. Bukreyev, J. E. CroweJr., E. O. Saphire, *Nat. Commun.* **2019**, *10*, 1788.

[8] a) H. A. Elshabrawy, M. M. Coughlin, S. C. Baker, B. S. Prabhakar, *PLoS ONE* **2012**, *7*, e50366; b) M. Yuan, N. C. Wu, X. Zhu, C. D. Lee, R. T. Y. So, H. Lv, C. K. P. Mok, I. A. Wilson, *Science* **2020**, *368*, 630.

[9] M. Knossow, J. J. Skehel, *Immunology* **2006**, *119*, 1.

[10] a) J. R. Whittle, R. Zhang, S. Khurana, L. R. King, J. Manischewitz, H. Golding, P. R. Dormitzer, B. F. Haynes, E. B. Walter, M. A. Moody, T. B. Kepler, H. X. Liao, S. C. Harrison, *Proc. Natl. Acad. Sci. USA* **2011**, *108*, 14216; b) Y. Iba, Y. Fujii, N. Ohshima, T. Sumida, R. Kubota-Koketsu, M. Ikeda, M. Wakiyama, M. Shirouzu, J. Okada, Y. Okuno, Y. Kurosawa, S. Yokoyama, *J. Virol.* **2014**, *88*, 7130; c) D. D. Raymond, G. Bajic, J. Ferdman, P. Suphaphiphat, E. C. Settembre, M. A. Moody, A. G. Schmidt, S. C. Harrison, *Proc. Natl. Acad. Sci. USA* **2018**, *115*, 168; d) A. Watanabe, K. R. McCarthy, M. Kuraoka, A. G. Schmidt, Y. Adachi, T. Onodera, K. Tonouchi, T. M. Caradonna, G. Bajic, S. Song, C. E. McGee, G. D. Sempowski, F. Feng, P. Urick, T. B. Kepler, Y. Takahashi, S. C. Harrison, G. Kelsoe, *Cell* **2019**, *177*, 1124.

[11] T. Bizebard, B. Gigant, P. Rigolet, B. Rasmussen, O. Diat, P. Bosecke, S. A. Wharton, J. J. Skehel, M. Knossow, *Nature* **1995**, *376*, 92.

[12] a) C. Barbey-Martin, B. Gigant, T. Bizebard, L. J. Calder, S. A. Wharton, J. J. Skehel, M. Knossow, *Virology* **2002**, *294*, 70; b) J. Sui, W. C. Hwang, S. Perez, G. Wei, D. Aird, L. M. Chen, E. Santelli, B. Stec, G. Cadwell, M. Ali, H. Wan, A. Murakami, A. Yammanuru, T. Han, N. J. Cox, L. A. Bankston, R. O. Donis, R. C. Liddington, W. A. Marasco, *Nat. Struct. Mol. Biol.* **2009**, *16*, 265.

[13] N. L. Kallewaard, D. Corti, P. J. Collins, U. Neu, J. M. McAuliffe, E. Benjamin, L. Wachter-Rosati, F. J. Palmer-Hill, A. Q. Yuan, P. A. Walker, M. K. Vorlaender, S. Bianchi, B. Guarino, A. De Marco, F. Vanzetta, G. Agatic, M. Foglierini, D. Pinna, B. Fernandez-Rodriguez, A. Fruehwirth, C. Silacci, R. W. Ogrodowicz, S. R. Martin, F. Sallusto, J. A. Suzich, A. Lanzavecchia, Q. Zhu, S. J. Gamblin, J. J. Skehel, *Cell* **2016**, *166*, 596.

[14] I. G. Denisov, Y. V. Grinkova, A. A. Lazarides, S. G. Sligar, *J. Am. Chem. Soc.* **2004**, *126*, 3477.

[15] E. S. Salnikov, C. Aisenbrey, G. Anantharamaiah, B. Bechinger, *Chem. Phys. Lipids* **2019**, *219*, 58.

[16] A. O. Oluwole, J. Klingler, B. Danielczak, J. O. Babalola, C. Vargas, G. Pabst, S. Keller, *Langmuir* **2017**, *33*, 14378.

[17] T. H. Bayburt, J. W. Carlson, S. G. Sligar, *J. Struct. Biol.* **1998**, *123*, 37.

[18] R. Kuai, L. J. Ochyl, K. S. Bahjat, A. Schwendeman, J. J. Moon, *Nat. Mater.* **2017**, *16*, 489.

[19] a) B. Kong, S. Moon, Y. Kim, P. Heo, Y. Jung, S. H. Yu, J. Chung, C. Ban, Y. H. Kim, P. Kim, B. J. Hwang, W. J. Chung, Y. K. Shin,

B. L. Seong, D. H. Kweon, *Nat. Commun.* **2019**, *10*, 185; b) H. Oh, Y. Jung, S. Moon, J. Hwang, C. Ban, J. Chung, W.-J. Chung, D.-H. Kweon, *ACS Appl. Mater. Interfaces* **2021**, *13*, 36757.

[20] P. Bhattacharya, S. Grimme, B. Ganesh, A. Gopisetty, J. R. Sheng, O. Martinez, S. Jayarama, M. Artinger, M. Meriggioli, B. S. Prabhakar, *J. Virol.* **2010**, *84*, 361.

[21] W. L. DeLano, M. H. Ultsch, A. M. de Vos, J. A. Wells, *Science* **2000**, *287*, 1279.

[22] T. J. White, T. Bruns, S. Lee, J. Taylor, *PCR Protoc.: Guide Methods Appl.* **1990**, *18*, 315.

[23] L. Shi, Q. T. Shen, A. Kiel, J. Wang, H. W. Wang, T. J. Melia, J. E. Rothman, F. Pincet, *Science* **2012**, *335*, 1355.

[24] a) D. Alford, H. Ellens, J. Bentz, *Biochemistry* **1994**, *33*, 1977; b) T. Stegmann, I. Bartoldus, J. Zumbrunn, *Biochemistry* **1995**, *34*, 1825.

[25] a) I. G. Denisov, B. J. Baas, Y. V. Grinkova, S. G. Sligar, *J. Biol. Chem.* **2007**, *282*, 7066; b) T. K. Ritchie, Y. V. Grinkova, T. H. Bayburt, I. G. Denisov, J. K. Zolnerciks, W. M. Atkins, S. G. Sligar, *Methods Enzymol.* **2009**, *464*, 211; c) A. K. Harris, J. R. Meyerson, Y. Matsuoka, O. Kuybeda, A. Moran, D. Bliss, S. R. Das, J. W. Yewdell, G. Sapiro, K. Subbarao, S. Subramaniam, *Proc. Natl. Acad. Sci. USA* **2013**, *110*, 4592.

[26] Y. V. Grinkova, I. G. Denisov, S. G. Sligar, *Protein Eng. Des. Sel.* **2010**, *23*, 843.

[27] a) J. Miehling, D. Goricanec, F. Hagn, *ChemBioChem* **2018**, *19*, 1927; b) M. L. Nasr, G. Wagner, *Curr. Opin. Struct. Biol.* **2018**, *51*, 129; c) Y. Yusuf, J. Massiot, Y. T. Chang, P. H. Wu, V. Yeh, P. C. Kuo, J. Shiue, T. Y. Yu, *Langmuir* **2018**, *34*, 3525.

[28] A. J. Stevens, Z. Z. Brown, N. H. Shah, G. Sekar, D. Cowburn, T. W. Muir, *J. Am. Chem. Soc.* **2016**, *138*, 2162.

[29] a) L. Zhang, H. Shen, Y. Gong, X. Pang, M. Yi, L. Guo, J. Li, S. Arroyo, X. Lu, S. Ovchinnikov, G. Cheng, X. Liu, X. Jiang, S. Feng, H. Deng, *Chem. Sci.* **2019**, *10*, 3271; b) J. T. Sockolosky, S. Kivimae, F. C. Szoka, *PLoS One* **2014**, *9*, e102566; c) W. Choe, T. A. Durgannavar, S. J. Chung, *Materials* **2016**, *9*, 994.

[30] K. Welsher, S. P. Sherlock, H. Dai, *Proc. Natl. Acad. Sci. USA* **2011**, *108*, 8943.

[31] P. J. Wyatt, *Anal. Chim. Acta* **1993**, *272*, 1.

[32] G. Dekkers, A. E. Bentlage, T. C. Stegmann, H. L. Howie, S. Lissenberg-Thunnissen, J. Zimring, T. Rispens, G. Vidarsson, *mAbs* **2017**, *9*, 767.

[33] M. B. Overdijk, S. Verploegen, A. O. Buijsse, T. Vink, J. H. Leusen, W. K. Bleeker, P. W. Parren, *J. Immunol.* **2012**, *189*, 3430.

[34] A. O. Hassan, J. B. Case, E. S. Winkler, L. B. Thackray, N. M. Kafai, A. L. Bailey, B. T. McCune, J. M. Fox, R. E. Chen, W. B. Alsoussi, *Cell* **2020**, *182*, 744.

[35] L. Gui, K. K. Lee, in *Influenza Virus*, Springer, New York **2018**, p. 261.

[36] a) L. D. Hernandez, L. R. Hoffman, T. G. Wolfsberg, J. M. White, *Annu. Rev. Cell Dev. Biol.* **1996**, *12*, 627; b) R. F. Epand, J. C. Macosko, C. J. Russell, Y. K. Shin, R. M. Epand, *J. Mol. Biol.* **1999**, *286*, 489.

[37] a) S. Biswas, S. R. Yin, P. S. Blank, J. Zimmerberg, *J. Gen. Physiol.* **2008**, *131*, 503; b) S. Boonstra, J. S. Blijleven, W. H. Roos, P. R. Onck, E. van der Giessen, A. M. van Oijen, *Annu. Rev. Biophys.* **2018**, *47*, 153.

[38] a) C. Cruz-Teran, K. Tiruthani, M. McSweeney, A. Ma, R. Pickles, S. K. Lai, *Adv. Drug Delivery Rev.* **2021**, *169*, 100; b) W. F. Dall'Acqua, P. A. Kiener, H. Wu, *J. Biol. Chem.* **2006**, *281*, 23514; c) T. K. Hart, R. M. Cook, P. Zia-Amirhosseini, E. Minthorn, T. S. Sellers, B. E. Maleeff, S. Eustis, L. W. Schwartz, P. Tsui, E. R. Appelbaum, *J. Allergy Clin. Immunol.* **2001**, *108*, 250.

[39] a) H. Wu, D. S. Pfarr, S. Johnson, Y. A. Brewah, R. M. Woods, N. K. Patel, W. I. White, J. F. Young, P. A. Kiener, *J. Mol. Biol.* **2007**, *368*, 652; b) C. Wegzyn, L. K. Toh, G. Notario, S. Biguenet, K. Unnebrink, C. Park, D. Makari, M. Norton, *Infect. Dis. Ther.* **2014**, *3*, 133; c) A. Tang, Z. Chen, K. S. Cox, H.-P. Su, C. Callahan, A. Fridman, L. Zhang, S. B. Patel, P. J. Cejas, R. Swoyer, S. Touch, M. P. Citron, D. Govindarajan, B. Luo, M. Eddins,

**ADVANCED
SCIENCE NEWS**

www.advancedsciencenews.com

**small
methods**

www.small-methods.com

J. C. Reid, S. M. Soisson, J. Galli, D. Wang, Z. Wen, G. J. Heidecker, D. R. Casimiro, D. J. DiStefano, K. A. Vora, *Nat. Commun.* **2019**, *10*, 4153.

[40] S. O. Ali, T. Takas, A. Nyborg, K. Shoemaker, N. L. Kallewaard, R. Chiong, F. Dubovsky, R. M. Mallory, *Antimicrob. Agents Chemother.* **2018**, *62*, e00694.

[41] a) G. Nakamura, N. Chai, S. Park, N. Chiang, Z. Lin, H. Chiu, R. Fong, D. Yan, J. Kim, J. Zhang, W. P. Lee, A. Estevez, M. Coons, M. Xu, P. Lupardus, M. Balazs, L. R. Swem, *Cell Host Microbe* **2013**, *14*, 93; b) J. M. McBride, J. J. Lim, T. Burgess, R. Deng, M. A. Derby, M. Maia, P. Horn, O. Siddiqui, D. Sheinson, H. Chen-Harris, *Antimicrob. Agents Chemother.* **2017**, *61*, e01154.

[42] a) D. F. Robbiani, C. Gaebler, F. Muecksch, J. C. C. Lorenzi, Z. Wang, A. Cho, M. Agudelo, C. O. Barnes, A. Gazumyan, S. Finkin, T. Hägglöf, T. Y. Oliveira, C. Viant, A. Hurley, H.-H. Hoffmann, K. G. Millard, R. G. Kost, M. Cipolla, K. Gordon, F. Bianchini, S. T. Chen, V. Ramos, R. Patel, J. Dizon, I. Shimeliovich, P. Mendoza, H. Hartweger, L. Nogueira, M. Pack, J. Horowitz, et al., *Nature* **2020**, *584*, 437; b) J. Hansen, A. Baum, K. E. Pascal, V. Russo, S. Giordano, E. Wloga, B. O. Fulton, Y. Yan, K. Koon, K. Patel, *Science* **2020**, *369*, 1010; c) X. Chen, R. Li, Z. Pan, C. Qian, Y. Yang, R. You, J. Zhao, P. Liu, L. Gao, Z. Li, Q. Huang, L. Xu, J. Tang, Q. Tian, W. Yao, L. Hu, X. Yan, X. Zhou, Y. Wu, K. Deng, Z. Zhang, Z. Qian, Y. Chen, L. Ye, *Cell. Mol. Immunol.* **2020**, *17*, 647.

[43] M. B. Fessler, *Clin. Exp. Allergy* **2012**, *42*, 340.

[44] M. Numata, Y. V. Grinkova, J. R. Mitchell, H. W. Chu, S. G. Sligar, D. R. Voelker, *Int. J. Nanomed.* **2013**, *8*, 1417.

[45] A. B. Sigalov, L. J. J. C. Stern, P. O. lipids, *Chem. Phys. Lipids* **2001**, *113*, 133.